DOI: 10.2478/eces-2025-0028 ECOL CHEM ENG S. 2025;32(4):535-556

Nadia MEKKAS[1], Soulef AZIZI[1,2], Selahattin YILMAZ[3], Mohammed BENBOUZID[1,2]
Günsev DIZOĞLU[3], Hana TAIB[1] and Noureddine GHERRAF[4*]

N-FORMYLATION OF AMINES OVER A PROTONIC ZEOLITE SOCONY MOBIL (H-ZSM-5) AND ION-EXCHANGED ZEOLITE: CATALYTIC PERFORMANCE AND REUSABILITY

Abstract: An efficient and sustainable method was developed for the N-formylation of primary and secondary amines using formic acid in dichloromethane at room temperature over zeolite H-ZSM-5 and ion-exchanged forms (Zn-ZSM-5, Cu-ZSM-5, Ag-ZSM-5, and Cd-ZSM-5). The catalysts were characterised by X-ray diffraction (XRD), scanning electron microscopy (SEM), Brunauer-Emmett-Teller (BET) surface area, ammonia temperature-programmed desorption (NH_3-TPD), and inductively coupled plasma-optical emission spectrometry (ICP-OES) analyses, revealing a regular hexagonal plate-like morphology and high surface area. H-ZSM-5 exhibited the largest surface area (248.2 m^2/g) and total acidity (0.109 mmol NH_3/g), while ion exchange slightly modified these properties. The catalytic system achieved excellent yields (up to 99 %) for various amines, demonstrating high efficiency and reusability. This study highlights the potential of zeolite-based catalysts as effective, recyclable materials for N-formylation processes.

Keywords: H-ZSM-5, ion-exchanged, N-formylation, formic acid, acidity

Introduction

The protection of reactive amino groups via formylation, achieved through the attachment of formyl (-CHO) groups to generate amides, constitutes a fundamental transformation in organic synthesis [1]. This process, known as the formylation of amines, is highly important in synthetic organic chemistry because of its versatility and wide-ranging applications. Formamides, the products of this reaction, are highly valued for their dual role as key intermediates in the synthesis of natural products and as building blocks in pharmaceutical and synthetic applications [2]. Notable examples include their

[1] Laboratory of Analytical Sciences, Materials and Environment (LASME), Larbi Ben M'Hidi University, 04000, Oum El Bouaghi, Algeria, email: nadia.mekkas@univ-oeb.dz, hannatayeb0@gmail.com, ORCID: NM 0009-0004-5404-7012, HT 0009-0001-0981-9712
[2] Laboratory of Sciences and Technology of the Environment, Constantine University, Constantine, Algeria, email: azizi_soulef@yahoo.fr, benbouzidm97@gmail.com, ORCID: SA 0000-0001-6893-6858, MB 0000-0002-3299-6733
[3] Department of Chemical Engineering, Izmir Institute of Technology, Izmir, Turkey, email: selahattinyilmaz@iyte.edu.tr, gunsevdizoglu@iyte.edu.tr, ORCID: SY 0000-0003-2853-0751, GD 0000-0002-2419-7114
[4] Laboratory of Natural Resources and Management of Sensitive Environments, University of Oum El Bouaghi, Algeria, ORCID: 0000-0002-9635-2275
[*] Corresponding author: ngherraf@yahoo.com

involvement in the synthesis of fluoroquinolones [3], 1, 2-dihydroquinolones [4], nitrogen-based heterocyclic scaffolds [5], and substituted aryl imidazoles [6]. In addition to their role as intermediates, formamides serve as protective groups for the nitrogen functionality in amines, facilitating selective transformations in multistep synthetic sequences. Moreover, they exhibit catalytic properties as Lewis bases, playing pivotal roles in various organic transformations, such as allylation reactions, the synthesis of acid chlorides from carboxylic acids, the hydrosilylation of carbonyl compounds, and peptide synthesis, where they function as nitrogen-protecting groups [7, 8]. These diverse applications underscore the critical importance of efficient and reliable methodologies for the formylation of amines in modern organic synthesis. The synthesis of formamides has been extensively studied, and various reagents and methods have been employed to achieve this transformation. Notable examples include the use of acetic formic anhydride [9], chloral [10], activated formic acid with DCC [11] or EDCI [12], activated formic esters [13, 14], ammonium formate [15], and 2,2,2-trifluoroethyl formate [16]. Other reagents, such as zeolites [17], HCOOH with sodium formate, PEG-400, and polyvinyl alcohol, have also been explored [18-21]. Additionally, catalytic systems such as Na^{+}-montmorillonite [22], nanocerium oxide [23], silica-bonded N-propyl sulphamic acid [24], $TiCl_3$(OTF) [25], CDMT [26], and KF-Al_2O_3 [27] have been utilised. In addition, N-formylation of amines with other formylation reagents such as carbon dioxide (CO_2) [28-30]. However, these methods often suffer from significant limitations, including prolonged reaction times, elevated temperatures, the use of hazardous reagents, and tedious purification processes. Moreover, many of these approaches rely on homogeneous catalysts, which introduce additional challenges, such as difficulties in catalyst recovery and separation, the need for toxic solvents, and the environmental hazards associated with waste generation. These drawbacks severely restrict the scalability and industrial applicability of these methods [31]. The challenges posed by homogeneous catalysts have further underscored the need for alternative approaches that are efficient, safe, and environmentally benign [32, 33]. In this context, the development of heterogeneous catalytic systems has garnered considerable attention. In particular, heterogeneous solid acids have emerged as promising alternatives because of their environmental compatibility, nontoxic nature, reusability, simplified reaction workups, and enhanced reaction rates [34]. These features align with the principles of green chemistry and address many of the shortcomings of homogeneous systems. Recent advances in heterogeneous catalysis have highlighted the utility of material-supported and unsupported metal nanoparticles, attributed to their unique structures and exceptional catalytic efficiencies [32, 33, 35, 36]. Among heterogeneous catalysts, zeolites have proven to be particularly effective in facilitating organic transformations. These microporous crystalline materials often outperform traditional Lewis acid catalysts because of their high stability, tunable acidity, and structural versatility [37].

H-ZSM-5 is one of the most noteworthy zeolites in this context. This medium-pore zeolite, characterised by its 5.1 Å - 5.6 Å pores, features a three-dimensional channel system formed by 10-membered rings [38]. The high acidity, remarkable thermal stability, shape-selective behaviour, and large surface area of H-ZSM-5 make it a robust catalyst for a variety of organic reactions [39, 40]. Structurally, H-ZSM-5 is a crystalline microporous aluminosilicate in which aluminium atoms are incorporated into the framework, generating negative charges that are balanced by extra framework cations. When these cations are hydrogen ions, the material exhibits Brønsted acidity, a key property for catalytic applications. Hydrothermal treatments can further enhance its performance by introducing

Lewis acidity through the formation of extra framework aluminium species [41]. A notable advancement in zeolite synthesis involves the use of fluoride ions as mineralisers, which replace hydroxide ions, to enable synthesis under near-neutral conditions (pH ~5) [41, 42]. This method not only allows the direct formation of NH_4-ZSM-5, which can be converted to acidic H-ZSM-5 in a single calcination step but also produces zeolites with superior properties. Zeolites synthesised in fluoride media exhibit larger crystal sizes, higher crystallinity, and fewer silanol defects than those prepared in hydroxide media [43-47]. These characteristics make fluoride-synthesised zeolites, particularly H-ZSM-5, highly attractive for green and efficient catalytic processes in the synthesis of formamides and beyond.

In Cu zeolites, Cu^{2+} cations are incorporated into the zeolite framework and act as active sites for catalysing nitrogen oxides (NO_x) conversion [48]. The only exception is Cu^{2+}-exchanged Y-type zeolite, which was previously reported to exhibit low catalytic activity. However, Cu^{+}-exchanged ZSM-5 zeolites demonstrate exceptionally high and stable catalytic activity for NO decomposition, highlighting ZSM-5 as an excellent carrier for Cu^{2+} ions in catalytic decomposition reactions [49]. A notable example is their use in selective catalytic reduction of NO_x gases using ammonia (NH_3-SCR) [50, 51]. Additionally, studies have reported the preparation of Fe-ZSM-5 zeolites, but factors such as the incorporated Fe content, crystal size, and acid properties have not been fully explored. Larger Fe-ZSM-5 crystals, ranging from 400 nm to 600 nm in size, have also been fabricated [52]. El-Malki et al. [53] synthesised Zn/Ga/Fe-ZSM-5 zeolites loaded with acidic cations (Zn, Ga, and Fe) and studied their effect on Brønsted acid sites in ZSM-5. Coelho et al. [54] investigated how basic sodium ions influence the number and strength of acid sites. Using in situ FTIR spectroscopy with pyridine as a probe molecule, researchers determined the type, number, and strength of acid sites. The acidity of Mn^{+}-ZSM-5 follows the order Ba^{2+}-ZSM-5 < Ca^{2+}-ZSM-5 < NH_4^{+}-ZSM-5 < Al^{3+}-ZSM-5 < H^{+}-ZSM-5, which corresponds to the increasing acidity of the loaded cations: $Ba^{2+} < Ca^{2+} < NH_4^{+} < Al^{3+} < H^{+}$ [55]. Ion exchange plays a crucial role in modifying the acidic and catalytic properties of H-ZSM-5. By introducing alkali metal ions such as Li^{+}, Na^{+}, and Cs^{+} into the zeolite framework, the density and strength of Brønsted acid sites can be adjusted. This modification significantly impacts the selectivity and durability of the catalyst in methanol-to-olefin (MTO) reactions. For example, Cs^{+}-exchanged H-ZSM-5 has a lower hydrogen transfer index and greater propene selectivity than the parent zeolite [56]. Moreover, Ni-modified H-ZSM-5 zeolites demonstrate improved catalytic efficiency in hydrocracking and hydroisomerisation reactions, which is attributed to the synergistic interaction between Bronsted and Lewis acid sites. This modification enhances stability and selectivity, particularly in the transformation of long-chain alkanes [57]. Furthermore, nanosised CuO/H-ZSM-5 has been identified as an efficient, stable, and recyclable catalyst for formamide synthesis. The total acid amount in CuO/H-ZSM-5 is greater than that in H-ZSM-5, contributing to its superior catalytic performance [31].

In previous studies, several types of zeolites have been utilised in the N-formylation of amines, including natural HEU zeolite (2012) [58], Cu nanoparticles supported on natural natrolite zeolite (2015) [59], nanosised CuO/HZSM-5 (2016) [31], zeolite A along with its ion-exchanged forms (2017) [60], and palladium catalyst deposited over modified clinoptilolite zeolite (2021) [61]. In this study, new research for the N-formylation of primary (aniline, n-propylamine, tert-butylamine) and secondary amines (dipropylamine, pyrrolidine) with formic acid as an environmentally benign formylating reagent using

zeolite H-ZSM-5 and ion-exchanged forms (Zn-ZSM-5, Cu-ZSM-5, Ag-ZSM-5, Cd-ZSM-5) as catalysts in dichloromethane at room temperature for 4 h. The reaction scheme is illustrated in Figure 1.

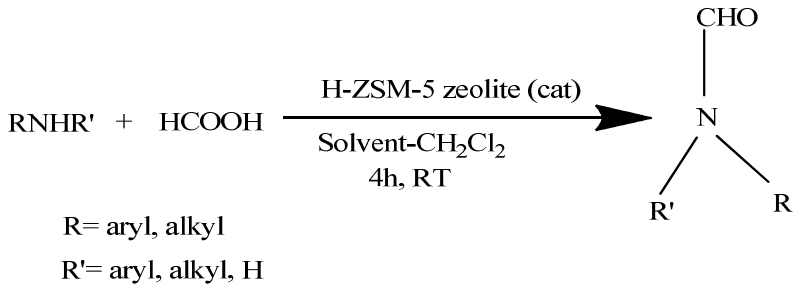

Fig. 1. N-formylation of amines using formic acid in the presence of zeolite H-ZSM-5 or ion-exchanged forms

Materials and methods

Materials

The materials used in the experimental study were as follows. Tetra propylammonium bromide (TPABr, 98 % purity) and tetraethyl orthosilicate (TEOS, 98 % purity) were obtained from Aldrich Chemistry. Sodium aluminate ($NaAlO_2$, 500 g), silver nitrate (purity ≥ 99 %), and n-propylamine (purity ≥ 98 %) were supplied by BIOCHEM-Chemopharma. Ammonium fluoride (NH_4F, purity ≥ 98 %), hydrofluoric acid (HF, purity ≥ 40 %), zinc nitrate hexahydrate (98 % purity), nitric acid (HNO_3, purity ≥ 65 %), dipropylamine (99 % purity), pyrrolidine (99 % purity), and tert-butylamine (98 % purity) were obtained from Sigma-Aldrich. Cadmium nitrate tetrahydrate (99 % purity), formic acid (HCOOH, purity 98 % - 100 %), and aniline (purity ≥ 99.5 %) were supplied by Merck. Copper(II) nitrate hemi-pentahydrate (98 % purity) was sourced from Alfa Aesar, while lithium tetraborate (98 % purity) was acquired from Fluka. Dichloromethane (CH_2Cl_2, purity ≥ 99.9 %) was obtained from Honeywell/Riedel-de Haen. Additionally, TLC silica gel 60 F_{245} was procured from Supelco-Sigma Aldrich, and capillary tubes were used for thin-layer chromatography (TLC) analysis.

Synthesis of H-ZSM-5

The synthesis of H-ZSM-5 zeolite was carried out through the preparation of a clear gel mixture. Initially, sodium aluminate ($NaAlO_2$), tetra propylammonium bromide (TPABr) as the structure-directing agent, and ammonium fluoride (NH_4F) were dissolved in distilled water at room temperature. Tetraethyl orthosilicate (TEOS) was then added as the silica source under vigorous stirring. The molar composition of the synthesis mixture was maintained at 0.07 TPABr: 1 TEOS: 0.012 $NaAlO_2$: 1.6 NH_4F: 80 H_2O. The pH was carefully adjusted to 7 using a few drops of hydrofluoric acid (HF) solution, and the mixture was aged for 3 hours to ensure complete homogenisation. The resulting gel was transferred to a Teflon-lined stainless-steel autoclave and subjected to hydrothermal crystallisation at 170 °C for 135 hours in the oven. After cooling to room temperature, the mother liquor exhibited a slightly acidic pH (4 - 5). The solid product was separated by

filtration, thoroughly washed with distilled water until neutral (pH = 7), and dried at 120 °C for 48 hours in the oven to yield the NH_4-ZSM-5 intermediate. Finally, the protonic form of the zeolite (H-ZSM-5) was obtained by calcination of the NH_4-ZSM-5 sample at 500 °C for 5 hours [41].

Preparation of ion-exchanged NH4-ZSM-5

The ion exchange was performed at ambient temperature by suspending 0.6 g of unmodified zeolite (NH_4-ZSM-5) in 30 mL aqueous solutions of metal nitrates ($Cu(NO_3)_2$, $Zn((NO_3)_2$, $Cd(NO_3)_2$, or $AgNO_3$) at a concentration of 0.1 mol/L. The mixtures were stirred continuously for 24 h to ensure complete ion exchange. Afterward, the resulting materials were filtered and washed thoroughly with distilled water until no residual nitrate ions were detected. Following overnight drying at 80 °C in the oven, the samples were calcined at 400 °C for 4 h to stabilise and activate the exchanged metal sites [62].

Synthesis for the N-formylation of amines

The catalytic N-formylation reactions were conducted at room temperature in a 50 mL round-bottom flask. Typically, 1.0 mmol of aniline was reacted with 1.2 mmol aqueous formic acid in the presence of 0.05 g of either H-ZSM-5 zeolite (or ion-exchanged forms) in 10 mL dichloromethane (CH_2Cl_2). The reaction mixtures were continuously stirred for 4 h [37, 59, 63]. Upon completion, indicated by thin-layer chromatography (TLC) monitoring with capillary tubes used for sample application under UV light (CN-6 lamp, 230 V, 50/60 Hz, 254 nm - 365 nm), the flask was cooled in an ice bath for 15 min. The catalyst was removed by filtration, and the filtrate was evaporated under reduced pressure to yield the purified formamide product. For catalyst recycling, the recovered catalyst was thoroughly washed with dichloromethane and dried prior to reuse in subsequent reaction cycles.

Characterisation of the synthesised formamide products was performed using spectroscopic techniques including proton nuclear magnetic resonance (^{1}H NMR), carbon nuclear magnetic resonance (^{13}C NMR), and attenuated total reflectance Fourier-transform infrared spectroscopy (ATR-FTIR). The product yield was calculated using the equation:

$$Yield = \left(\frac{\text{Actual mass of obtained product [g]}}{\text{Theoretical mass of product [g]}}\right) \cdot 100\ [\%] \quad (1)$$

The experimental product mass represents the actual amount of isolated product, while the theoretical product mass corresponds to the expected mass based on stoichiometric calculations. Repeated experiments confirmed consistent yields across multiple reaction cycles (Fig. 1), demonstrating excellent catalytic stability and recyclability.

Characterisation

The crystalline structures of the H-ZSM-5 zeolite and its ion-exchanged forms were analysed via X-ray diffraction (XRD) using a Philips X'Pert diffractometer equipped with Cu K_α radiation (λ = 1.5406 Å). Diffraction patterns were collected within the 2θ range of 5° to 80°, with incremental scanning steps of 0.02°. The instrumental error in 2θ measurement was ±0.02°, and peak intensity reproducibility was within ±1.0 %.

Scanning electron microscopy (SEM) analysis of the crystal sizes and morphologies was performed using a QUANTA FEG 250-FEI microscope. The measurement uncertainty

for particle size estimation was approximately ±5 %, while the spatial resolution of the SEM was 1 nm - 2 nm under high-vacuum mode.

The Brunauer-Emmett-Teller (BET) surface area and porosity measurements of zeolite samples were conducted using a Micromeritics 3 Flex Porosity Analyzer (version 6.02). Prior to analysis, approximately 0.2 g - 0.3 g of each sample was degassed at 300 °C for 3 hours under vacuum to remove adsorbed species. Nitrogen (N_2) adsorption-desorption isotherms were recorded at liquid nitrogen temperature (–196 °C). Specific surface areas were subsequently calculated using the linearised form of the BET equation, with an estimated error of ±2 % for surface area and ±3 % for total pore volume.

Temperature-Programmed Desorption of Ammonia (NH_3-TPD) was performed using a Micromeritics AutoChem II Chemisorption Analyzer. A 150 mg catalyst sample was placed in a quartz tube and its temperature was increased to 500 °C at a ramp rate of 5 °C/min and held for 3 h under 50 mL/min He flow. It was then cooled to 100 °C, followed by exposure to 50 mL/min of NH_3/He for 30 min. Physically adsorbed NH_3 was removed by switching to He flow (100 mL/min) for 3 h. Desorption was conducted by heating at 10 °C/min under 50 mL/min He up to 500 °C and held for 30 min. The TCD signal TCD signal was recorded, with a temperature accuracy of ±1°C and desorption peak area reproducibility within ±3 %.

Elemental composition analysis was carried out via Inductively Coupled Plasma-Optical Emission Spectroscopy (ICP-OES) using an Agilent Technologies 5110 instrument. Samples were prepared by fusion dissolution: 0.05 g of sample was mixed with 0.5 g lithium tetraborate in a platinum crucible and fused at 1000 °C for 1 hour. The resultant glass bead was dissolved in 1.6 M nitric acid (HNO_3) using magnetic stirring, and the solution volume was adjusted to 62.5 mL [64]. Dilution was performed as necessary to reach suitable analyte concentrations. The Limit of Detection (LOD) for most elements was ~0.01 mg/L, and the precision of ICP-OES analysis was typically ±2 % Relative Standard Deviation (RSD).

Catalytic reaction products were characterised by Attenuated Total Reflectance Fourier-Transform Infrared (ATR-FTIR) spectroscopy and Nuclear Magnetic Resonance (^{1}H NMR and ^{13}C NMR). NMR spectra were recorded using a Bruker Ascend 400 MHz spectrometer equipped with a Broadband Fluorine Observation (BBFO) probe optimised for liquid samples. Samples for NMR analysis were prepared by dissolving 5 mg - 10 mg of purified product in 500 µL deuterated chloroform $CDCl_3$ (containing 0.03 % tetramethylsilane (TMS) as an internal standard). Chemical shifts (δ) are reported in parts per million (ppm) relative to TMS, and coupling constants (J) in Hertz [Hz]. The accuracy of chemical shift measurements was ±0.001 ppm for ^{1}H and ±0.01 ppm for ^{13}C NMR.

ATR-FTIR spectra were acquired using a Bruker ALPHA spectrometer with OPUS 6.5 software, covering the spectral range of 4000 cm^{-1} - 400 cm^{-1} with a resolution of 2 cm^{-1}. Each spectrum represents an average of 32 scans in transmittance mode. The wavenumber precision of the instrument was ±0.01 cm^{-1}, and absorbance reproducibility was within ±1 %. Samples for FTIR analysis were prepared by mixing with the NMR solvent deuterated chloroform ($CDCl_3$) and applied directly onto the ATR crystal for immediate spectral acquisition.

Results and discussion

XRD analysis

Figure 2 displays the X-ray diffraction (XRD) patterns of zeolite H-ZSM-5 and the ion-exchanged forms. All the forms exhibit a crystalline character devoid of any amorphous phase. The diffraction patterns obtained in the 2θ ranges of 7° - 9° and 20° - 25° match the known diffraction pattern for ZSM-5 [65]. Most of the peaks observed in zeolite H-ZSM-5 are present in equal amounts in the variations in the metal ion exchange of the zeolite. These observations indicate that the zeolite ZSM-5 framework remains structurally unchanged when exposed to various metal ions and maintains its crystallinity [63]. These results confirm the purity of the ZSM-5 zeolite and highlight the distinctive characteristics of the MFI structure, verifying that its crystallinity is well maintained.

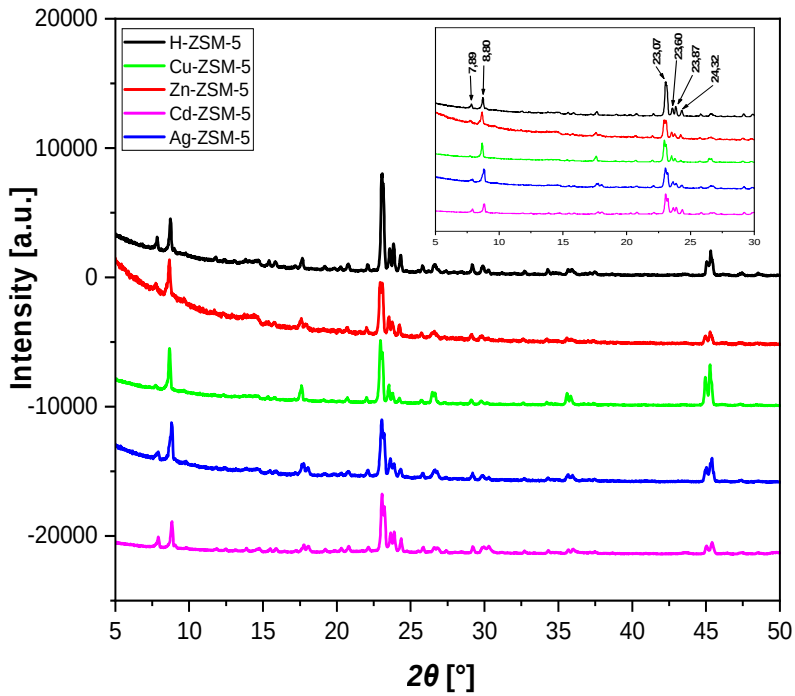

Fig. 2. X-ray diffraction patterns of zeolite H-ZSM-5 and the ion-exchanged forms

SEM analysis

Figure 3 shows scanning electron microscopy (SEM) images of zeolite H-ZSM-5, which indicate the typical prismatic crystal morphology of this material. The crystals have a regular plate-like morphology with a hexagonal shape and an elongated form, with widths of approximately 5 µm - 9 µm and lengths of about 40 µm - 50 µm. Compared with those produced in alkaline environments, the crystals synthesised with fluoride have larger dimensions [41].

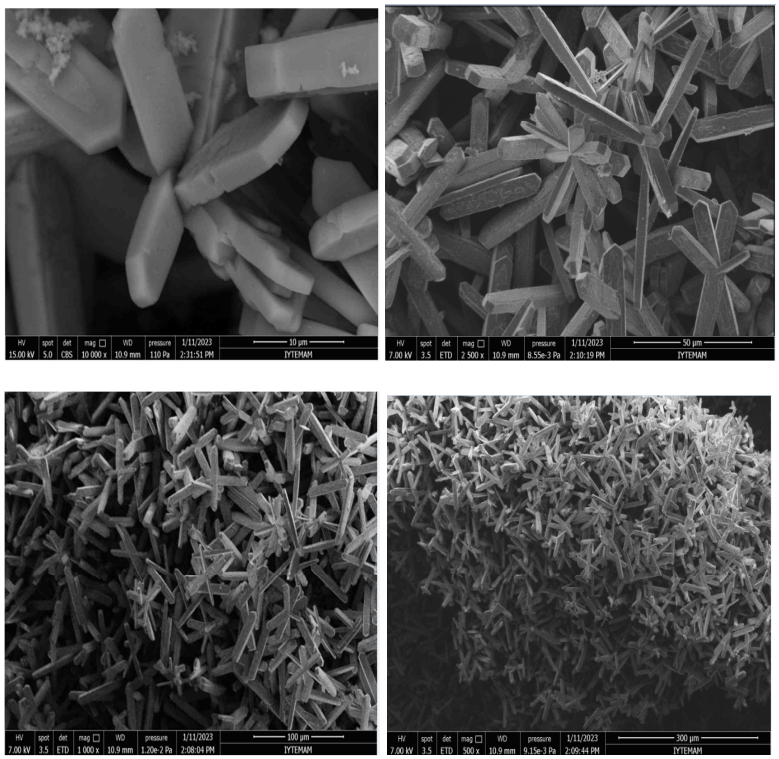

Fig. 3. Scanning electron microscopy (SEM) image of zeolite H-ZSM-5

BET analysis

The nitrogen adsorption/desorption isotherms presented in Figure 4 reveal that all samples, including H-ZSM-5 and its ion-exchanged forms (Cu-ZSM-5, Zn-ZSM-5, Ag-ZSM-5, and Cd-ZSM-5), exhibit type IV isotherm hysteresis loops, which are typical of materials containing both mesoporous and microporous structures [66, 67]. This indicates that while ZSM-5 possesses intrinsic microporosity, the ion-exchange process introduces additional mesoporosity due to partial structural modifications or pore blockage by metal cations.

Table 1 provides a detailed summary of the surface and volume properties of these catalysts, which were calculated via the BET method for surface area and the BJH method for pore volume distribution. Among the studied samples, the H-ZSM-5 catalyst exhibits the highest specific surface area (248.20 m^2/g) and micropore area (178.60 m^2/g), representing 82.47 % microporosity, which reflects its predominantly microporous crystalline framework. Its total pore volume (0.097 cm^3/g) and narrow median pore width (1.563 Å) further confirm the well-ordered microporous structure characteristic of pure ZSM-5 [41].

Upon ion exchange, a remarkable decrease in surface area and microporosity is observed, which can be attributed to the introduction of metal ions (Cu^{2+}, Zn^{2+}, Ag^{+}, Cd^{2+}) into the zeolite framework. These ions may occupy or block micropores, thereby reducing

accessibility and generating secondary mesoporosity. For example, Cu-ZSM-5 shows a drastic drop in surface area (16.28 m^2/g) and microporosity (20 %), along with a substantial increase in mesoporosity (80 %) and a larger pore width (7.372 Å), indicating structural modification and partial loss of microporous order.

Similarly, Zn-ZSM-5 displays an extremely low microporosity (5 %) with a wide pore diameter (6.338 Å), suggesting that zinc ions cause severe pore blocking or framework distortion. In contrast, Ag-ZSM-5 maintains moderate microporosity (60 %) despite its low surface area, implying that silver ions induce less structural disruption. The Cd-ZSM-5 sample shows intermediate behaviour, with a balanced contribution of microporosity (33.33 %) and mesoporosity (66.67 %), suggesting partial preservation of the zeolite's pore network.

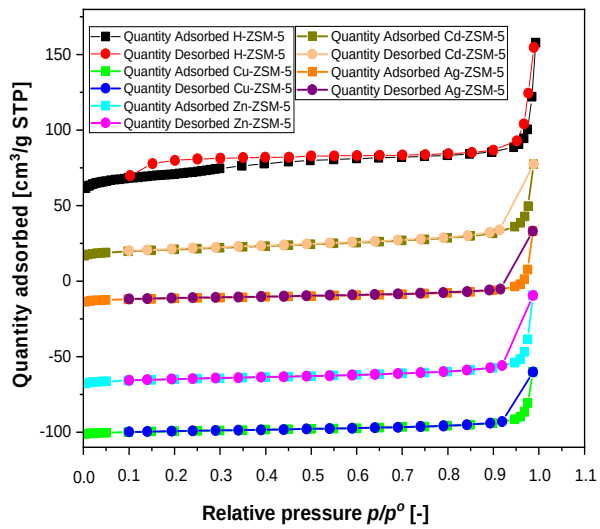

Fig. 4. Nitrogen adsorption-desorption isotherms of the H-ZSM-5 zeolite and ion-exchanged forms

Table 1

Surface and volume properties of H-ZSM-5 zeolite and ion-exchanged samples calculated from BET analysis

Samples	S_{BET} [a] [m^2/g]	S_{Micro} [m^2/g]	S_{Ext} [m^2/g]	V_{micro} [b] [cm^3/g]	V_{meso} [c] [cm^3/g]	V_{Total} [d] [cm^3/g]	Micro [e] [%]	Meso [f] [%]	d [g] [Å]
H-ZSM-5	248.20	178.60	69.60	0.080	0.017	0,097	82.47	17.53	1.563
Cu-ZSM-5	16.28	3.36	12.92	0.0006	0.0024	0.003	20	80	7.372
Zn-ZSM-5	16.39	0.59	15.80	0.0002	0.0038	0.004	5	95	6.338
Ag-ZSM-5	17.58	7.94	9.64	0.003	0.002	0.005	60	40	5.897
Cd-ZSM-5	28.83	6.14	22.69	0.003	0.006	0.009	33.33	66.67	5.241

a: Total surface area calculated using the BET method
b: Micropore volume ($V_{mi}c_{ro}$) determined by the t-plot method
c: Mesopore volume (V_{meso}) calculated as $V_{total} - V_{mi}c_{ro}$
d: Total pore volume estimated from nitrogen adsorption at $p/p°$ = 0.0100 for pores < 9.384 Å
e: Microporosity = $V_{mi}c_{ro} / V_{total} \cdot 100$ [%]
f: Mesoporosity = $V_{meso} / V_{total} \cdot 100$ [%]
g: Median pore width determined by the Horvath-Kawazoe method

Overall, these results demonstrate that ion exchange substantially modifies the textural properties of ZSM-5, influencing pore size distribution, surface area, and the micro-mesoporous balance. The extent of these changes depends on the nature, charge, and ionic radius of the exchanged metal cations, which affect of the zeolite framework [66, 67].

For example, Miskolczi et al. [68] employed a different preparation method for synthesising ZSM-5 and its ion-exchanged forms, obtaining a specific surface area of 356 m^2/g for H-ZSM-5 and 268 m^2/g for Zn-ZSM-5. This indicates that the synthesis and ion-exchange procedures have a significant influence on the resulting textural properties, and different preparation routes can therefore lead to considerable variations in surface area and porosity of the zeolite materials.

ICP-OES analysis

The inductively Coupled Plasma-Optical Emission Spectroscopy (ICP-OES) analysis results for the zeolite H-ZSM-5 and its ion-exchanged forms are summarised in Table 2. The data clearly illustrate the variations in both the Si/Al ratio and the metal ion content after ion exchange. The weight percentages of the incorporated metal ions were determined to be 0.06 % wt. for Cu-ZSM-5, 0.06 % wt. for Cd-ZSM-5, 0.03 % wt. for Ag-ZSM-5, and 0.03 % wt. for Zn-ZSM-5.

The Si/Al ratio of the H-ZSM-5 was found to be 115.8, and it increased slightly in all ion-exchanged samples, reaching the highest value of 127.5 for Zn-ZSM-5. This gradual increase in the Si/Al ratio may be attributed to a slight dealumination of the zeolite framework that occurs during the ion-exchange process.

Overall, the ICP-OES results confirm the successful incorporation of metal ions into the zeolite and suggest minor structural modifications associated with dealumination during the ion-exchange treatment [69-71].

Table 2

ICP-OES results and total acidity of zeolite H-ZSM-5 and ion-exchanged forms

Catalysts	Ratio Si/Al	Metal ions [% wt.]	Total acidity [mmol $NH_3/g_{catalyst}$]
H-ZSM-5	115.8	/	0.109
Cu-ZSM-5	119.6	0.06	0.122
Cd-ZSM-5	121.6	0.06	0.145
Ag-ZSM-5	124.2	0.03	0.115
Zn-ZSM-5	127.5	0.03	0.125

TPD analysis

The acidic properties of both the zeolite H-ZSM-5 and ion-exchanged forms were investigated using ammonia temperature-programmed desorption (NH_3-TPD), as shown in Figure 5. The obtained TPD profiles exhibit two main desorption regions: one between 100 °C - 300 °C, attributed to NH_3 molecules adsorbed on weak acid sites, and the other between 300 °C - 500 °C, associated with NH_3 molecules adsorbed on strong acid sites, which are crucial for catalytic activity [64, 72, 73]. The metal ion-exchange process significantly enhanced both the number of strong acid sites and the overall acidity of the catalysts. The total acidity (mmol NH_3/g catalyst), as summarised in Table 2, increased in the following order: H-ZSM-5 < Ag-ZSM-5 < Cu-ZSM-5 < Zn-ZSM-5 < Cd-ZSM-5. These findings clearly demonstrate that the acidity of H-ZSM-5 increases as a function of

the nature and amount of the exchanged metal ions, confirming the beneficial effect of metal incorporation on the surface acidity of the zeolite.

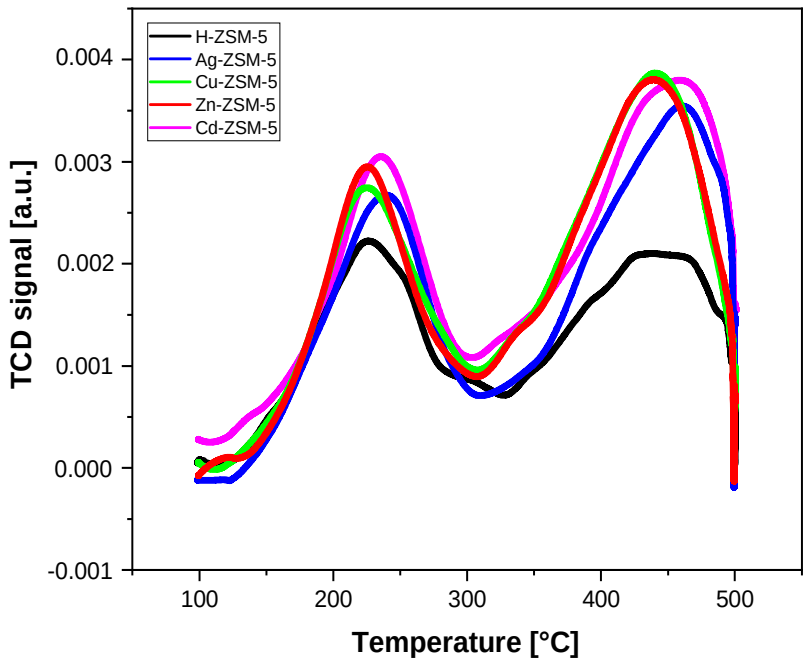

Fig. 5. NH_3-TPD profiles of zeolite H-ZSM-5 and the ion-exchanged forms

ATR-FTIR and NMR analysis

N-phenylformamide (1)

The product N-phenyl formamide was isolated as a dark brown oil. Comprehensive characterisation via ATR-FTIR spectroscopy revealed distinct functional group vibrations: a pronounced absorption at 3266 cm^{-1} associated with the N–H stretching vibration, a strong and sharp absorption band at 1675 cm^{-1} corresponding to the carbonyl (C=O) stretching mode, and characteristic C–H stretching vibrations manifesting as weak-to-medium intensity bands in the region of 3160 cm^{-1} - 2700 cm^{-1}. Multiple sharp bands within the range of 1599 cm^{-1}, 1542 cm^{-1}, 1491 cm^{-1}, 1442 cm^{-1}, and 1402 cm^{-1} were observed, indicative of aromatic C=C stretching vibrations. Additionally, bending vibrations for aromatic C–H appeared in the region of 940 cm^{-1} - 620 cm^{-1}, while absorption bands at 1311 cm^{-1} - 1252 cm^{-1} were attributed to C–N stretching vibrations [1].

Detailed structural elucidation by NMR spectroscopy provided further validation. The ^1H NMR spectrum (400 MHz, $CDCl_3$) exhibited resonances at δ 9.13 (d, J = 8.7 Hz, 1H, formyl proton), δ 8.66-8.50 (m, 2H, aromatic protons), δ 8.16 (d, J = 1.8 Hz, 1H, aromatic proton), δ 7.42 (d, J = 7.7 Hz, 2H), δ 7.20-7.12 (m, 4H), and δ 7.05-6.92 (m, 4H, aromatic protons). The ^{13}C NMR spectrum (400 MHz, $CDCl_3$) revealed carbon resonances at δ 162.23 (carbonyl carbon), δ 158.99, 136.10, 135.85,

128.63, 127.96, 124.17, 123.68, 119.23, and 117.73, confirming aromatic carbon. All analytical data closely aligned with previously reported literature values [1, 74-77].

The catalytic efficacy for N-phenyl formamide synthesis was remarkably high, demonstrating yields of 89 % (Ag-ZSM-5), 93 % (Cd-ZSM-5), 95 % (Cu-ZSM-5), 97 % (Zn-ZSM-5), and a superior 99 % yield with zeolite H-ZSM-5. Notably, catalyst recyclability was confirmed by consistent catalytic performance over three consecutive reuse cycles, further underscoring catalyst stability and efficiency (Table 3).

Table 3

N-formylation of amines using H-ZSM-5 and ion exchange forms in formic acid at room temperature under 10 mL of solvent-dichloromethane conditions[a]

Entry	Formic acid	Amines	Product	Time [h]	(H-ZSM-5)[b] Yield[c] [%]	Ag-ZSM-5)[b] Yield[c] [%]	Cu-ZSM-5)[b] Yield[c] [%]	Zn-ZSM-5)[b] Yield[c] [%]	Cd-ZSM-5)[b] Yield[c] [%]
1	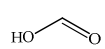	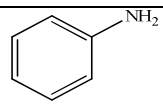 Aniline	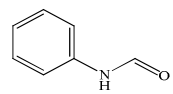 N-Phenyl formamide	4	99	89	95	97	93
2	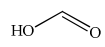	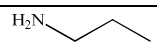 n-Propylamine	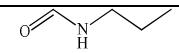 n,n-Propyl formamide	4	98	87	94	96	91
3	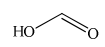	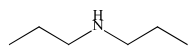 Dipropylamine	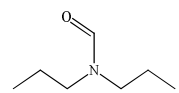 n,n-Dipropyl formamide	4	97	86	93	95	90
4	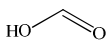	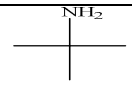 tert-butylamine	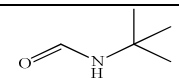 n-tert-butyl formamide	4	96	85	92	94	88
5	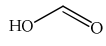	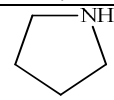 Pyrrolidine	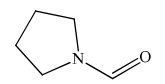 Pyrrolidine-1-carbaldehyde	4	92	80	88	90	84

[a]Reaction conditions: amine (1.0 mmol), formic acid (1.2 mmol) and [b]catalyts (0.05 g). [c]Yield refers to the pure isolated product. Yield after the three cycles. Yield calculated using eq. (1)

N, N-propylformamide (2)

The product N,N-propylformamide was obtained as a dark yellow oil, comprehensively characterised by ATR-FTIR spectroscopy. The spectrum displayed notable absorption bands: a prominent peak at 3398 cm^{-1} from N–H stretching vibrations, a sharp carbonyl (C=O) stretching absorption at 1580 cm^{-1}, and C–H stretching vibrations spanning 3120 cm^{-1} - 2600 cm^{-1}. Distinct absorption bands at

1464 cm^{-1}, 1376 cm^{-1}, and 1343 cm^{-1} were assigned to bending vibrations of C–H bonds in the propyl groups. Additional characteristic vibrations from the propyl chain, including CH_2 and CH_3 rocking, wagging, and twisting motions, were identified at 1050 cm^{-1}, 922 cm^{-1}, 761 cm^{-1}, 731 cm^{-1}, 695 cm^{-1}, and 643 cm^{-1}. A significant band observed at 1205 cm^{-1} corresponded to C–N stretching vibrations.

NMR spectral data provided further structural confirmation. The ^1H NMR spectrum (400 MHz, $CDCl_3$) exhibited signals at δ 8.27 (s, 1H, formyl proton), δ 3.36 (s, 1H, amine proton), δ 2.65 (s, 2H), δ 1.47 (d, J = 7.1 Hz, 2H, methylene protons), and δ 0.75 (d, J = 6.8 Hz, 3H, methyl protons). Correspondingly, the ^{13}C NMR spectrum (400 MHz, $CDCl_3$) revealed resonances at δ 169.02 (carbonyl carbon), 40.92, 20.96, and 10.88, characteristic of propyl group carbon environments. These analytical results aligned precisely with literature values [75].

Catalytic performance analysis demonstrated high product yields: 87 % (Ag-ZSM-5), 91 % (Cd-ZSM-5), 94 % (Cu-ZSM-5), 96 % (Zn-ZSM-5), and an optimal 98 % with zeolite H-ZSM-5. The catalytic stability and efficiency were robustly maintained across three reuse cycles, confirming excellent reusability and sustained catalytic activity (Table 3).

N,N-Dipropylformamide (3)

The product N,N-Dipropylormamide isolated as a yellow oil, exhibited characteristic ATR-FTIR absorption bands: a prominent carbonyl stretching vibration at 1560 cm^{-1} and extensive C–H stretching vibrations within the range of 3200-2600 cm^{-1}. Characteristic bending vibrations associated with C–H bonds in propyl chains appeared at 1464 cm^{-1}, 1376 cm^{-1}, and 134 cm^{-1}, alongside specific bands corresponding to CH_2 and CH_3 rocking, wagging, and twisting vibrations at 1049 cm^{-1}, 912 cm^{-1}, 764 cm^{-1}, 734 cm^{-1}, 644 cm^{-1}, and 453 cm^{-1}. A distinctive C–N stretching vibration was observed at 1204 cm^{-1}.

The structure was further verified by NMR spectroscopy. The ^1H NMR spectrum (400 MHz, $CDCl_3$) displayed signals at δ 7.86 (s, 1H, formyl proton), δ 2.33-2.12 (m, 4H, methylene protons), δ 1.09 (dq, J = 15.1, 7.5 Hz, 4H, additional methylene protons), and δ 0.31 (t, J = 7.5 Hz, 6H, methyl protons). ^{13}C NMR spectrum resonances appeared at δ 167.70 (carbonyl carbon), 48.66, 18.98, and 10.71, corroborating the expected carbon environments of the dipropyl group. Reaction yields were notably high: 86 % (Ag-ZSM-5), 90 % (Cd-ZSM-5), 93 % (Cu-ZSM-5), 95 % (Zn-ZSM-5), and an exceptional 97 % yield using zeolite H-ZSM-5. Consistent results across three reuse cycles reinforced the stability and practicality of the catalyst (Table 3).

N-tert-butyl formamide (4)

The product N-tert-butyl formamide was obtained as a white crystalline solid. Its structure was thoroughly confirmed using ATR-FTIR spectroscopy, which demonstrated characteristic absorptions corresponding to its functional groups. Notable bands included a prominent N-H stretching vibration at 3402 cm^{-1}, and a distinct carbonyl (C=O) stretching peak at 1571 cm^{-1}. C–H stretching vibrations were observed within the range of 3190 cm^{-1} - 2500 cm^{-1}. Furthermore, bending vibrations characteristic of the tert-butyl group appeared distinctly at 1404 cm^{-1}, 1377 cm^{-1}, 1344 cm^{-1}, and 1309 cm^{-1}. Additionally, rocking and wagging vibrations of C–H bonds

in the tert-butyl moiety manifested at 909 cm^{-1}, 763 cm^{-1}, 729 cm^{-1}, 644 cm^{-1}, and 456 cm^{-1}. A sharp band at 1223 cm^{-1} was assigned to C–N stretching.

NMR spectroscopic analyses further validate the structure. The ^{1}H NMR spectrum (400 MHz, $CDCl_3$) exhibited resonances at δ 8.23 (s, 1H, formyl proton), δ 1.57 (s, 1H), and δ 1.06 (s, 9H, tert-butyl protons). Correspondingly, the ^{13}C NMR spectrum (400 MHz, $CDCl_3$) revealed resonances at δ 168.62 (carbonyl carbon), 51.06, and 27.41, clearly consistent with the tert-butyl functional groups. Product formation and structural identity were fully consistent with literature standards. The catalytic performance for synthesising N-tert-butyl formamide yielded robust results: 85 % (Ag-ZSM-5), 88 % (Cd-ZSM-5), 92 % (Cu-ZSM-5), 94 % (Zn-ZSM-5), and an impressive 96 % yield with zeolite H-ZSM-5. Catalytic stability was confirmed by consistent yields across three consecutive catalytic cycles, highlighting excellent catalyst durability and efficiency (Table 3).

Pyrrolidine-1-carbaldehyde (5)

The product pyrrolidine-1-carbaldehyde was isolated as a dark brown solid. ATR-FTIR spectroscopy provided detailed characterisation, identifying essential functional groups. Notable absorptions included a sharp C=O stretching vibration at 1733 cm^{-1} and distinct C–H stretching vibrations at 2923 cm^{-1} and 2852 cm^{-1}. Additional C–H bending vibrations appeared prominently at 1589 cm^{-1}, 1458 cm^{-1}, 1378 cm^{-1}, 1345 cm^{-1}, 1165 cm^{-1}, 1078 cm^{-1}, 1031 cm^{-1}, and 760 cm^{-1}, with a clear C–N stretching vibration at 1244 cm^{-1}.

Structural verification by NMR spectroscopy provided clear evidence of product identity. The ^{1}H NMR spectrum (400 MHz, $CDCl_3$) exhibited resonances at δ 8.47 (s, 1H, formyl proton), δ 3.16 (s, 4H, methylene protons adjacent to nitrogen), and δ 1.91 (s, 4H, methylene protons distal to nitrogen). The corresponding ^{13}C NMR spectrum showed resonances at δ 169.18 (carbonyl carbon), 44.62, and 24.43. Analytical data aligned well with previously reported literature [37, 75]. Catalytic evaluations yielded improved outcomes compared to previously published methodologies, with yields of 80 % (Ag-ZSM-5), 84 % (Cd-ZSM-5), 88 % (Cu-ZSM-5), 90 % (Zn-ZSM-5), and 92 % using zeolite H-ZSM-5. Catalyst recyclability was demonstrated through three reuse cycles without significant performance loss, underscoring catalyst robustness (Table 3).

Comparative catalytic evaluation

In this study, we developed a new approach for the activation of formic acid (HCOOH) as an N-formylating agent using zeolite H-ZSM-5 and ion-exchanged forms (Cu-ZSM-5, Zn-ZSM-5 Ag-ZSM-5, and Cd-ZSM-5) as heterogeneous catalysts. The reactions were carried out at room temperature in dichloromethane, providing the desired formamide products in excellent yields.

Among the available formylating agents, formic acid is particularly attractive because it is inexpensive, stable, non-volatile, non-flammable, and tolerant to moisture. Unlike other agents, it can be safely stored and handled. Conventional methods for N-formylation with aqueous formic acid typically require high temperatures, prolonged reaction times, and a Dean-Stark trap under reflux in toluene. Therefore, the development of efficient, mild, and economical N-formylation methods remains an active area of research.

Table 4

Comparison of the current methodology with previously reported methods for the N-formylation of amines (aniline, n-propylamine, dipropylamine, tert-butylamine and pyrrolidine) of amines using H-ZSM-5 and ion exchange forms in formic acid at room temperature under 10 mL of solvent-dichloromethane conditions

Amines	**Formylating method**	**Solvent**	**T [°C]**	**Time**	**Yield [%]**	**Ref.**
Aniline	Ammonium formate (HCO_2NH_4)	CH_3CN	Reflux	11 h	96	[15]
Aniline	HCOOH, SSA	Solvent-free	50-60	7 min	99	[78]
Aniline	HCOOH, HEU zeolite	Solvent-free	R.T*	30 min	91.88	[37]
Aniline	HCOOH, Natrolite zeolite/Cu NPs	Solvent-free	R.T	17 min	95	[59]
Aniline	HCOOH, CuO/HZSM-5	Solvent-free	R.T	15 min	96	[31]
Aniline	HCOOH, [Bmim]BF4	ultrasonic irradiation	R.T	15 min	99	[1]
Aniline	HCOOH, zeolite A	Solvent-free	R.T	25 min	90	[63]
Aniline	H_2O_2, Na_2SO_3, chromium	CH_3OH	80	2 h	85	[79]
Aniline	CO_2,$PhSiH_3$, Xanthone, DTPA	DMSO	R.T	48 h	82.6	[80]
Aniline	HCOOH, H-ZSM5 zeolite	CH_2Cl_2	R.T	4 h	99	This work
Aniline	HCOOH, Ag-ZSM5 zeolite	CH_2Cl_2	R.T	4 h	89	This work
Aniline	HCOOH, Cu-ZSM5 zeolite	CH_2Cl_2	R.T	4 h	95	This work
Aniline	HCOOH, Zn-ZSM5 zeolite	CH_2Cl_2	R.T	4 h	97	This work
Aniline	HCOOH, Cd-ZSM5 zeolite	CH_2Cl_2	R.T	4 h	93	This work
n-propylamine	H_2O_2, Na_2SO_3, chromium	CH_3OH	80	2 h	75	[79]
n-propylamine	HCOOH, H-ZSM5 zeolite	CH_2Cl_2	R.T	4 h	98	This work
n-propylamine	HCOOH, Ag-ZSM5 zeolite	CH_2Cl_2	R.T	4 h	87	This work
n-propylamine	HCOOH, Cu-ZSM5 zeolite	CH_2Cl_2	R.T	4 h	94	This work
n-propylamine	HCOOH, Zn-ZSM5 zeolite	CH_2Cl_2	R.T	4 h	96	This work
n-propylamine	HCOOH, Cd-ZSM5 zeolite	CH_2Cl_2	R.T	4 h	91	This work
Dipropylamine	CO_2,$PhSiH_3$, Xanthone, DTPA	DMSO	R.T	48 h	88.5	[80]
Dipropylamine	HCOOH, H-ZSM5 zeolite	CH_2Cl_2	R.T	4 h	97	This work
Dipropylamine	HCOOH, Ag-ZSM5 zeolite	CH_2Cl_2	R.T	4 h	86	This work
Dipropylamine	HCOOH, Cu-ZSM5 zeolite	CH_2Cl_2	R.T	4 h	93	This work
Dipropylamine	HCOOH, Zn-ZSM5 zeolite	CH_2Cl_2	R.T	4 h	95	This work
Dipropylamine	HCOOH, Cd-ZSM5 zeolite	CH_2Cl_2	R.T	4 h	90	This work
Tert-butylamine	HCOOH, H-ZSM5 zeolite	CH_2Cl_2	R.T	4 h	96	This work
Tert-butylamine	HCOOH, Ag-ZSM5 zeolite	CH_2Cl_2	R.T	4 h	85	This work
Tert-butylamine	HCOOH, Cu-ZSM5 zeolite	CH_2Cl_2	R.T	4 h	92	This work
Tert-butyamine	HCOOH, Zn-ZSM5 zeolite	CH_2Cl_2	R.T	4 h	94	This work
Tert-butyamine	HCOOH, Cd-ZSM5 zeolite	CH_2Cl_2	R.T	4 h	88	This work
Pyrrolidine	HCOOH, HEU zeolite	Solvent-free	R.T	50 min	76	[37]
Pyrrolidine	CO_2, $PhSiH_3$, Xanthone, DTPA	DMSO	R.T	48 h	45.2	[80]
Pyrrolidine	HCOOH, H-ZSM5 zeolite	CH_2Cl_2	R.T	4 h	92	This work
Pyrrolidine	HCOOH, Ag-ZSM5 zeolite	CH_2Cl_2	R.T	4 h	80	This work
Pyrrolidine	HCOOH, Cu-ZSM5 zeolite	CH_2Cl_2	R.T	4 h	88	This work
Pyrrolidine	HCOOH, Zn-ZSM5 zeolite	CH_2Cl_2	R.T	4 h	90	This work
Pyrrolidine	HCOOH, Cd-ZSM5 zeolite	CH_2Cl_2	R.T	4 h	84	This work

* R.T - room temperature

Encouraged by the promising results under our reaction conditions, we explored the generality of this method by applying it to a range of primary (aniline, n-propylamine, tert-butylamine) and secondary (dipropylamine, pyrrolidine) amines. We then compared the catalytic efficiency of zeolite H-ZSM-5 and ion-exchanged forms. For the model reaction between aniline and formic acid (Fig. 1), the product yield was only 28 % without catalyst after 4 h of stirring. In contrast, the addition of 0.05 g of catalyst dramatically improved the outcome, affording yields of 89 % (Ag-ZSM-5), 93 % (Cd-ZSM-5), 95 % (Cu-ZSM-5), 97 % (Zn-ZSM-5), and up to 99 % with zeolite H-ZSM-5. These results highlight the critical role of the catalyst in promoting the reaction. Comparative results are presented in Figure 6 and Table 3.

The method was further extended to aromatic (aniline), aliphatic (n-propylamine, dipropylamine, and tert-butylamine), and heterocyclic (pyrrolidine) amines, all of which afforded N-formylated products in good to excellent yields (Table 3). Notably, pyrrolidine-1-carbaldehyde, previously reported with a 76 % yield [37], was obtained in significantly higher yields with our system: 80 % (Ag-ZSM-5), 84 % (Cd-ZSM-5), 88 % (Cu-ZSM-5), 90 % (Zn-ZSM-5), and 92 % using zeolite H-ZSM-5 (Table 4). Similarly, N, N-propylformamide, previously reported in 75 % yield [79], reached 87 % - 98 % under our catalytic conditions. Importantly, no side products were detected during the reactions, and open-chain aliphatic amines such as n-propylamine, dipropylamine, and tert-butylamine also reacted efficiently.

Compared with reported methods, which often suffer from high energy input, toxic or expensive reagents, homogeneous catalysts (difficult to recover), long reaction times, or undesired by-products, our system avoids these drawbacks. The process operates under mild, room-temperature conditions with an environmentally benign, recyclable, and reusable heterogeneous catalyst, making it a green and practical alternative for N-formylation.

Catalyst recycling experiments demonstrated that zeolite H-ZSM-5 and ion-exchanged forms retained high activity after three consecutive runs without requiring regeneration (Table 3). Zeolite H-ZSM-5 consistently gave the best results, with yields of 92 % for pyrrolidine-1-carbaldehyde, 96 % for N-tert-butylformamide, 97 % for N,N-dipropylformamide, 98 % for N,N-propylformamide, and 99 % for N-phenylformamide. The catalytic activity followed the order:

Zeolite H-ZSM-5 > Zn-ZSM-5 > Cu-ZSM-5 > Cd-ZSM-5 > Ag-ZSM-5,

while substrate reactivity followed the trend:

aniline > n-propylamine > dipropylamine > tert-butylamine > pyrrolidine.

The structures of all products were confirmed by ^{1}H-NMR, ^{13}C-NMR, ATR-FTIR, and TLC analyses. FTIR spectra clearly distinguished amines from formamides through the appearance of the characteristic C=O stretching band of formamides.

A plausible mechanism is outlined in Figure 7. The catalytic role of zeolite H-ZSM-5 and ion-exchanged forms is attributed to their Lewis acidity, which promotes activation of the carbonyl group in formic acid. The catalyst surface likely coordinates with the carbonyl oxygen, increasing the electrophilicity of the carbonyl carbon. This facilitates nucleophilic attack by the amine, followed by elimination of water, ultimately producing the corresponding formamide.

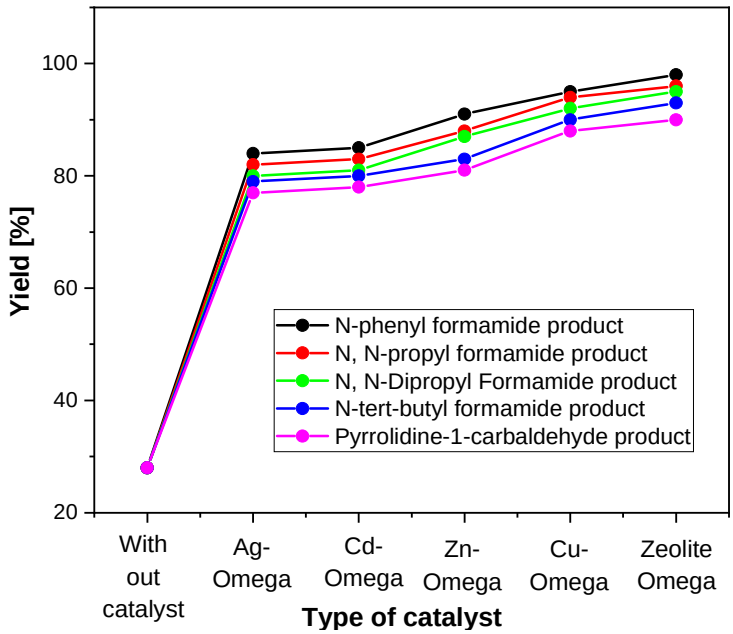

Fig. 6. Effect of catalytic efficiency of zeolite H-ZSM-5 and ion-exchanged forms (Cu-ZSM-5, Zn-ZSM-5, Cd-ZSM-5, and Ag-ZSM-5) on the N-formylation of amines. Reaction conditions: amine (1.0 mmol), formic acid (1.2 mmol), and catalyst (0.05 g) at room temperature in dichloromethane as solvent. Yields correspond to the pure isolated products. Reported yields are after the third catalytic cycle (see Table 3)

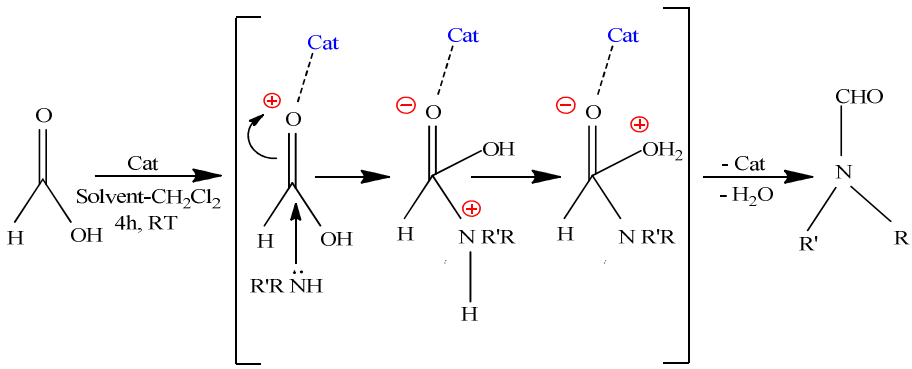

Catalyst (Cat): Zeolite H-ZSM -5 and ion-exchanged forms (Cu-ZSM-5, Zn-ZSM-5, Ag-ZSM-5 and Cd-ZSM-5).

Fig. 7. Mechanism of the zeolite H-ZSM-5 or ion-exchanged forms catalysed N-formylation of amines with formic acid (HCOOH)

Catalyst recyclability

The catalyst recycling is a crucial step, as it lowers the overall process cost and enhances sustainability. The recyclability of zeolite H-ZSM-5 and ion-exchanged

forms (Cu-ZSM-5, Zn-ZSM-5 Ag-ZSM-5, and Cd-ZSM-5) was evaluated for the N-formylation of amines under room-temperature conditions in dichloromethane for 4 h. After each reaction, the catalyst was separated by filtration, and the filtrate was evaporated under reduced pressure to afford the purified formamide product. The recovered catalyst was then washed thoroughly with dichloromethane, dried, and reused in subsequent reaction cycles. Each catalyst was successfully recycled up to three times without significant loss of activity, as shown in Figure 8, confirming their high stability and turnover under the applied conditions. To verify the heterogeneous nature of the catalysis, the filtrates obtained after each cycle were analysed by XRD (Fig. 9). The XRD results demonstrated that the catalysts remained structurally intact and fully active up to the third cycle, confirming their stability and safety during the reaction.

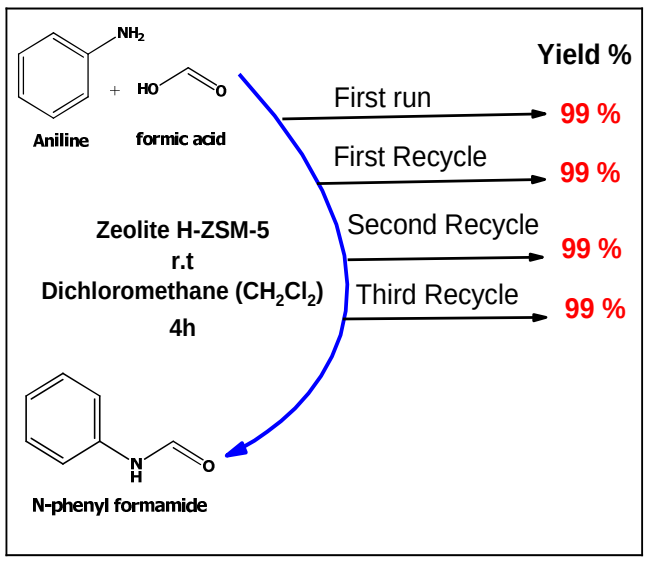

Fig. 8. Reusability of zeolite H-ZSM-5 as a catalyst for the N-formylation of aniline

Conclusion

In conclusion, we have developed a sustainable, efficient, and straightforward catalytic protocol for the N-formylation of primary (aniline, n-propylamine, tert-butylamine) and secondary (dipropylamine, pyrrolidine) amines using formic acid as a formylating agent. Zeolite H-ZSM-5 and ion-exchanged forms (Cu-ZSM-5, Zn-ZSM-5, Ag-ZSM-5, and Cd-ZSM-5) proved to be highly effective heterogeneous catalysts, delivering excellent performance under mild conditions in dichloromethane at room temperature. Comprehensive characterisation by XRD, SEM, BET surface area analysis, ICP-OES, and NH_3-TPD confirmed their structural integrity, high porosity and strong acidity. The catalysts were readily recovered by simple filtration and reused for up to three consecutive cycles without any noticeable loss of activity. The catalytic system demonstrated consistently high efficiency across diverse reactions. Zeolite H-ZSM-5

exhibited the best performance, achieving outstanding yields of 92 % for pyrrolidine-1-carbaldehyde, 96 % for N-tert-butylformamide, 97 % for N,N-dipropylformamide, 98 % for N,N-propylformamide, and 99 % for N-phenylformamide. The catalytic activity trend followed the order: Zeolite H-ZSM-5 > Zn-ZSM-5 > Cu-ZSM-5 > Cd-ZSM-5 > Ag-ZSM-5. Similarly, the reactivity order of amines across all catalysts was: aniline > n-propylamine > dipropylamine > tert-butylamine > pyrrolidine. The identities of the synthesised products were fully confirmed by ^{1}H NMR, ^{13}C NMR, ATR-FTIR spectroscopy, and thin-layer chromatography (TLC). Overall, this catalytic methodology offers multiple advantages, including operational simplicity, short reaction times, excellent yields, recyclability, and environmental compatibility. These features highlight the practical and sustainable potential of this approach, establishing it as a valuable strategy for the preparation of formamides in modern organic synthesis.

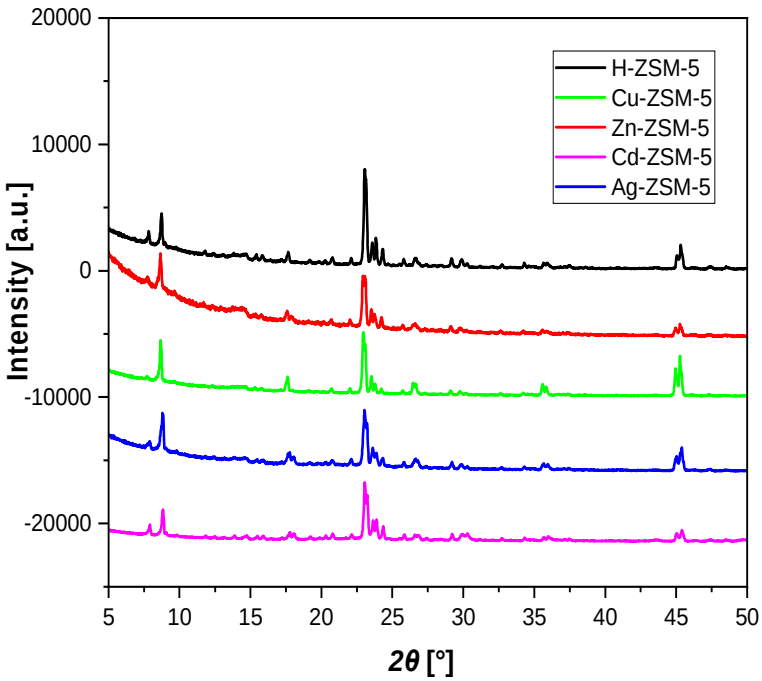

Fig. 9. X-ray diffraction (XRD) patterns of zeolite H-ZSM-5 and ion-exchanged forms after third recycle

References

[1] Kamble VT, Bondle GM, Pisal PM. Arab J Chem. 2017;10(1):S2436-42. DOI: 10.1016/j.arabjc.2013.09.007.
[2] Yang S, Cho A, Cho JH, Kim BM. Nanomaterials. 2021;11(8):2101. DOI:10.3390/nano11082101.
[3] Jackson A, Meth-Cohn O. J Chem Soc Chem Commun. 1995;(13):1319. DOI: 10.1039/c39950001319.
[4] Kobayashi K, Nagato S, Kawakita M, Morikawa O, Konishi H. Chem Lett. 1995;24(7):575-6. DOI: 10.1246/cl.1995.575
[5] Kakehi A, Ito S, Hayashi S, Fujii T. BCSJ. 1995;68(12):3573-80. DOI: 10.1246/bcsj.68.3573
[6] Chen BC, Bednarz MS, Zhao R, Sundeen JE, Chen P, Shen Z, et al. Tetrahedron Lett. 2000;31(41):5453-6. DOI: 10.1016/S0040-4039(00)00910-2.

[7] Downie IM, Earle MJ, Heaney H, Shuhaibar KF. Tetrahedron. 1993;24(37):4015-34: DOI: 10.1016/S0040-4020(01)89915-4.
[8] Martinez J, Laur J. Synthesis. 1982;1982(12):979-81. DOI:10.1055/s-1982-30034.
[9] Strazzolini P, Giumanini G, Cauci S. Tetrahedron. 1990;46(4):1081-118. DOI: 10.1016/S0040-4020(01)86676-X.
[10] Blicke FF, Lu C-J. J Am Chem Soc. 1952;74(15):3933-4. DOI: 10.1021/ja01135a503.
[11] Waki M, Meienhofer J Org Chem. 1977 May 27;42(11):2019-20. DOI: 10.1021/jo00431a046.
[12] Chen FMF, Benoiton NL. Synthesis. 1979;1979(10):709-10. DOI: 10.1055/s-1979-28805.
[13] Yale H. J Org Chem. 1971;36(21):3238-40. DOI: 10.1021/jo00820a603.
[14] Duczek W, Deutsch J, Vieth S, Niclas H-J. Synthesis. 1996;1996(1):37-8. DOI: 10.1055/s-1996-4153.
[15] Reddy PG, Kumar GKD, Baskaran S. Tetrahedron Lett. 2000;41(47):9149-51. DOI: 10.1016/S0040-4039(00)01636-1.
[16] Hill DR, Hsiao C-N, Kurukulasuriya R, Wittenberger SJ. Org Lett. 2002;4(1):111-3. DOI: 10.1021/ol016976d.
[17] Habibi D, Nasrollahzadeh M, Sahebekhtiari H. J Mol Catal A Chem. 2013;378:148-55. DOI: 10.1016/j.molcata.2013.04.001.
[18] Das B, Krishnaiah M, Balasubramanyam P, Veeranjaneyulu B, Kumar DN. Tetrahedron Lett. 2008;49(14):2225-7. DOI: 10.1016/j.tetlet.2008.02.050.
[19] Hosseini-Sarvari M, Sharghi H. J Org Chem. 2006;71(17):6652-4. DOI: 10.1021/jo060847z.
[20] Shekhar AC, Kumar AR, Sathaiah G, Paul VL, Sridhar M, Rao PS. Tetrahedron Lett. 2009;41(12):7099-101. DOI: 10.1016/j.tetlet.2009.10.006.
[21] Fard MR, Akhlaghinia B, Rezazadeh S. J Indian Chem Soc. 2015;92(10):1715-28. DOI: 10.1002/chin.201626065.
[22] Shirini F, Seddighi M, Mamaghani M. RSC Adv. 2014;4(92):50631-8. DOI: 10.1039/C4RA08282F.
[23] Sajadi SMS, Maham M, Rezaei A. Lett. Org. Chem. 2014;11(1):49-54. DOI: 10.2174/157017861131000057.
[24] Niknam K, Saberi D. Tetrahedron Lett. 2009;50(37):5210-4. DOI: 10.1016/j.tetlet.2009.06.140.
[25] Firouzabadi H, Iranpoor N, Farahi S. J Mol Catal A Chem. 2008;289:61-8. DOI: 10.1016/j.molcata.2008.04.010.
[26] De Luca L, Giacomelli G, Porcheddu A, Salaris M. Synlett. 2004;14(2004):2570-2. DOI: 10.1055/s-2004-834788.
[27] Mihara M, Ishino Y, Minakata S, Komatsu M. Synthesis. 2003;15:2317-20. DOI: 10.1055/s-2003-41060.
[28] Hulla M, Laurenczy G, Dyson PJ. ACS Catal. 2018;8:10619-30. DOI: 10.1021/acscatal.8b03274.
[29] Yuan X, Zhou Q, Chen Y, Yang H-J, Jiang Q, Hu J, et al. J Carbon Res. 2024;10(3):62. DOI: 10.3390/c10030062.
[30] Zhou Q, Chen Y, Yuan X, Yang H-J, Jiang Q, Hu J, et al. Catalysts. 2024;14:492. DOI: 10.3390/catal14080492.
[31] Tajbakhsh M, Alinezhad H, Nasrollahzadeh M, Kamali TA. J Colloid Interface Sci. 2016;471:37-47. DOI: 10.1016/j.jcis.2016.02.062.
[32] Canali L, Sherrington DC. Chem Soc Rev. 1999;28(2):85-93. DOI: 10.1039/A806483K.
[33] Minakata S, Komatsu M. Chem Rev. 2009;109(2):711-24. DOI: 10.1021/cr8003955.
[34] Bindig R, Butt S, Hartmann I, Matthes M, Thiel C. Catalysts. 2012;2(2):223-43. DOI: 10.3390/catal2020223.
[35] Fang Q, Sun Q, Zhong R, Wang H, Qi J. Mater Today Chem. 2025;46:102770. DOI: 10.1016/j.mtchem.2025.102770.
[36] Ma Y, Wang B, Wang H, Zhao X, Zhao Y, Wu S, et al. Int J Hydrogen Energy. 2025;126:484-95. DOI: 10.1016/j.ijhydene.2025.03.364.
[37] Bahari S, Mohammadi-Aghdam B, Mohammad Sajadi S, Zeidali F. Bull Korean Chem Soc. 2012;33(7):2251-4. DOI: 10.5012/bkcs.2012.33.7.2251.
[38] Sang S, Chang F, Liu Z, He Ch, He J, Xu L. Catal Today. 2004;93-95:729-34. DOI: 10.1016/j.cattod.2004.06.091.
[39] Marques MDFV, Moreira SC. J Mol Catal A Chem. 2003;192:93-101. DOI: 10.1016/S1381-1169(02)00250-9.
[40] Zhao D, Ingelsten HH, Skoglundh M, Palmqvist A. J Mol Catal A Chem. 2006;249(1-2):13-22. DOI: 10.1016/j.molcata.2005.12.033.
[41] Louis B, Kiwi-Minsker L. Microporous Mesoporous Mater. 2004;74(1-3):171-8. DOI: 10.1016/j.micromeso.2004.06.016.
[42] Flanigen EM. Pure Appl Chem. 1980;52(9):2191-211. DOI: 10.1351/pac198052092191.

[43] Hariharan S, Palanichamy M, Murugesan V. Arab J Chem. 2013;25:2679-82. DOI: 10.14233/ajchem.2013.13638.
[44] Prodinger S, Shi H, Wang H, Derewinski MA, Lercher JA. Appl Catal B Environ. 2018;237:996-1002. DOI: 10.1016/j.apcatb.2018.06.065.
[45] Kalvachev Y, Jaber M, Mavrodinova V, Dimitrov L, Nihtianova D, Valtchev V. Microporous Mesoporous Mater. 2013;177:127-34. DOI: 10.1016/j.micromeso.2013.04.028.
[46] Nabavi MS, Zhou M, Mouzon J, Grahn M, Hedlund J. Microporous Mesoporous Mater. 2019;278:167-74. DOI: 10.1016/j.micromeso.2018.11.007.
[47] Ye Y, Yao M, Chen H, Zhang X. Catal Lett. 2020;150(5):1445-53. DOI: 10.1007/s10562-019-03040-x.
[48] Paolucci C, Parekh AA, Khurana I, Di Iorio JR, Li H, Caballero JDA, et al. J Am Chem Soc. 2016;138(18):6028-48. DOI: 10.1021/jacs.6b02651.
[49] Iwamoto M, Furukawa H, Mine Y, Uemura F, Mikuriya S, Kagawa S. J Chem Soc Chem Commun. 1986;(16):1272. DOI: 10.1039/C39860001272.
[50] Hua Z, Song H, Zhou C, Xin Q, Zhou F, Fan W, et al. Chem Eng J. 2023;473:145106. DOI: 10.1016/j.cej.2023.145106.
[51] Lin K, Feng X, Zhang N, Song K, Yao Y, Jiao R, et al. Sci China Chem. 2025;1-35. DOI: 10.1007/s11426-025-2713-x.
[52] Sun H, Hu J, Zhou J. J Fuel Chem Technol. 1999;27:121-5. Available from: https://www.scopus.com/pages/publications/0033121209?inward=
[53] El-Malki E-M, Sachtler WMH, Van Santen RA,. J Phys Chem B. 1999;103(23):4611-22. DOI: 10.1021/jp990116l.
[54] Coelho A, Costa L, Marques MM, Fonseca IM, Lemos MANDA, Lemos F. Appl Catal A Gen. 2012;413-414:183-91. DOI: 10.1016/j.apcata.2011.11.010.
[55] Wu W, Weitz E. Appl Surf Sci. 2014;316:405-15. DOI: 10.1016/j.apsusc.2014.07.194.
[56] Dyballa M, Obenaus U, Blum M, Dai W. Catal Sci Technol. 2018;8(17):4440-9. DOI: 10.1039/C8CY01032C.
[57] Wei Q, Zhang P, Liu X. Front Chem. 2020;8:586445. DOI: 10.3389/fchem.2020.586445.
[58] Bahari S, Mohammadi-Aghdam B, Mohammad Sajadi S, Zeidali F. Bull Korean Chem Soc. 2012;33(7):2251-4. DOI: 10.5012/bkcs.2012.33.7.2251.
[59] Nasrollahzadeh M, Sajadi SM, Hatamifard A. J Colloid Interface Sci. 2015;460:146-53. DOI: 10.1016/j.jcis.2015.08.040.
[60] Bhat S, Naikoo R, Tomar R, Bhat R, Malla M, Ganie J. Pharm Pharmacol Int J. 2017;5(4):00130. DOI: 10.15406/ppij.2017.05.00130.
[61] Amirsoleimani M, Khalilzadeh MA, Zareyee D. J Mol Struct. 2021;1225:129076. DOI: 10.1016/j.molstruc.2020.129076.
[62] Djeffal N, Benbouzid M, Boukoussa B, Sekkiou H, Bengueddach A. Mater Res Express. 2017;4(3):035504. DOI: 10.1088/2053-1591/aa6465.
[63] Bhat S, Naikoo R, Tomar R, Bhat RA, Malla MA, Ganie JA, et al. Pharm Pharmacol Int J. 2017;5(3):00130. DOI: 10.15406/ppij.2017.05.00130.
[64] Kilic E, Yilmaz S. Int J Chem React Eng. 2010;8:2430. DOI: 10.2202/1542-6580.2430.
[65] Rohayati, Krisnandi YK, Sihombing R. AIP Conf Proc. 2017;1904:030094. DOI: 10.1063/1.4991198.
[66] Sing KSW. Pure Appl Chem. 1985;57(4):603-19. DOI: 10.1351/pac198557040603.
[67] Ravandi R, Khoshbin R, Karimzadeh R. J Porous Mater. 2018;25(3):451-61. DOI: 10.1007/s10934-017-0457-3.
[68] Miskolczi N, Juzsakova T, Sója J. J Energy Inst. 2019;92(1):118-27. DOI: 10.1016/j.joei.2017.10.017.
[69] Caldeira VP, Santos AG, Pergher SB, Costa MJ, Araujo AS. Quim Nova. 2016;39(3):292-7. DOI: 10.5935/0100-4042.20160019.
[70] Niu XR, Li J, Zhang L, Lei ZT, Zhao XL, Yang CH. RSC Adv. 2017;7(80):50619-25. DOI: 10.1039/C7RA10771D.
[71] Niu X, Bai Y, Du YE, Qi H, Chen Y. R Soc Open Sci. 2022;9(3):211284. DOI: 10.1098/rsos.211284.
[72] Hernando H, Moreno I, Fermoso J, Ochoa-Hernández C, Pizarro P, Coronado JM, et al. Biomass Convers Biorefin. 2017;7(3):289-304. DOI: 10.1007/s13399-017-0266-6.
[73] Zhang HZ, Zhu XD, Gao YY, Zhu KK. Adv Mater Res. 2011;311-313:540-4. DOI: 10.4028/www.scientific.net/AMR.311-313.540.
[74] Yadav JK, Yadav P, Awasthi SK, Agarwal A. RSC Adv. 2020;10(69):41229-36. DOI: 10.1039/D0RA07476D.
[75] Dan D, Chen F, Zhao W, Yu H, Han S, Wei Y. Dalton Trans. 2021;50(1):90-4. DOI: 10.1039/D0DT03300F.
[76] Mutra MR, Dhandabani GK, Wang JJ. Adv Synth Catal. 2018;360(20):3960-8. DOI: 10.1002/adsc.201800783.

[77] Kumar A, Sharma P, Sharma N, Kumar Y, Mahajan D. RSC Adv. 2021;11(41):25777-87. DOI: 10.1039/D1RA04848A.
[78] Habibi D, Rahmani P, Akbaripanah Z. J Chem. 2013;2013:972960. DOI: 10.1155/2013/972960.
[79] Yu H, Wu Z, Wei Z. Commun Chem. 2019;2:1-7. DOI: 10.1038/s42004-019-0109-4.
[80] Yuan X, Zhou Q, Chen Y, Jang H-J, Jiang Q, Hu J, et al. J Carbon Res. 2024;10(3):62. DOI: 10.3390/c10030062.